



Article

# Study on the Ablation Behavior of High-Intensity Lasers in Vacuum

Heyan Gao <sup>1</sup>, Ying Wang <sup>1,\*</sup>, Jifei Ye <sup>1,\*</sup>, Bangdeng Du <sup>1</sup>, Diankai Wang <sup>1</sup>, Sai Li <sup>1</sup>, Qianqian Cui <sup>1</sup>, Sibo Wang <sup>2</sup> and Tengfei Zhang <sup>1</sup>

- State Key Laboratory of Advanced Space Propulsion Technology and Application, Space Engineering University, Beijing 101416, China; gaohy\_s@hgd.edu.cn (H.G.); bddu13s@alum.imr.ac.cn (B.D.); diankai@mail.ustc.edu.cn (D.W.); hebtulisai@163.com (S.L.); cui\_qqq@163.com (Q.C.); teng20200229@163.com (T.Z.)
- <sup>2</sup> Beijing Institute of Tracking and Telecommunications Technology, Beijing 100080, China; bosiwang1@163.com
- Correspondence: yingwang8971@163.com (Y.W.); yjf1981@163.com (J.Y.)

Abstract: Laser ablation has been extensively studied by researchers due to its high precision, high efficiency processing capabilities, and wide range of application potentials. However, in a vacuum environment, due to the complexity of experimental conditions, specific application scenarios, and interdisciplinary interferences, more in-depth research on the ablation behavior of high-intensity lasers in vacuum is still insufficient. In response to such issues, experiments were conducted on titanium alloy perforation using a nanosecond laser in a vacuum environment. The variations in ablation depth and volume as functions of pulse energy, pulse number, and defocus were investigated. Both the depth and volume ablation efficiencies were calculated, and the three-dimensional morphology of the ablation holes was captured. Additionally, the ablation plume was observed to support the research conclusions. The results indicate that within the number of high-intensity laser pulses, the ablation depth per pulse can be increased by more than four times, and the average ablation volume per pulse can reach 0.97 μm<sup>3</sup>/μJ. The enhanced sputtering of molten material during the multi-pulse laser ablation process in a vacuum environment is identified as the primary factor contributing to the increased ablation efficiency. With the advancement of science and technology and the growing demand for applications, this research is crucial for the further development of fields such as space exploration and technology, advanced manufacturing technology, and basic scientific research.

Keywords: high-intensity lasers; laser ablation; vacuum environment



Academic Editors: Ivan Galvão, Rui Manuel Leal and Gustavo H. S. F. L. Carvalho

Received: 18 December 2024 Revised: 10 January 2025 Accepted: 14 January 2025 Published: 16 January 2025

Citation: Gao, H.; Wang, Y.; Ye, J.; Du, B.; Wang, D.; Li, S.; Cui, Q.; Wang, S.; Zhang, T. Study on the Ablation Behavior of High-Intensity Lasers in Vacuum. *Appl. Sci.* **2025**, *15*, 848. https://doi.org/10.3390/ app15020848

Copyright: © 2025 by the authors. Licensee MDPI, Basel, Switzerland. This article is an open access article distributed under the terms and conditions of the Creative Commons Attribution (CC BY) license (https://creativecommons.org/licenses/by/4.0/).

# 1. Introduction

Since the invention of Q-switching technology, extensive research has been conducted on laser drilling technology [1–5]. To achieve higher-quality micropores, studies have examined the effects of laser parameters (such as pulse width [6], wavelength [7], laser power [8], and the temporal and spatial distribution of laser energy [9]) and auxiliary parameters (including assistive blowing [10], enhanced electromagnetic fields [11], and variations in environmental pressure) on parameters such as hole depth, surface morphology, and the depth-to-diameter ratio. The research results indicate that specific laser parameters, such as pulse width, energy density, and repetition rate, along with environmental conditions, including vacuum level and heat dissipation, are crucial for achieving high-quality micropores. For instance, shorter pulse widths help minimize the heat-affected zone, resulting in cleaner hole edges, while higher energy densities promote deeper ablation. Furthermore, a

vacuum environment reduces plasma shielding effects, thus improving ablation efficiency. These relationships underscore the importance of carefully selecting laser parameters and environmental conditions to optimize micropore quality [12].

Recently, research has identified material evaporation and melt injection as the primary mechanisms responsible for the formation of ablative holes. When the laser irradiates the material surface, it first induces localized melting, followed by the rapid evaporation of the material. At the moment of evaporation, the recoil pressure generated by the evaporating material becomes sufficiently strong to expel the molten material from the ablation hole [13,14].

Based on the aforementioned mechanism, studies have shown that, in terms of machining accuracy (which refers to the degree to which the dimensions, shape, position, and other parameters of the fabricated workpiece conform to the design specifications, reflecting the precision and consistency of the machining process and serving as a key indicator of manufacturing quality), the drilling accuracy (which refers to the degree of conformity between the actual holes produced and the design specifications during the laser drilling process) of nanosecond lasers is lower than that of femtosecond and picosecond lasers [15]. However, from the perspective of machining efficiency (which refers to the speed and productivity of completing drilling operations per unit of time), nanosecond lasers exhibit higher efficiency due to their higher output power. Additionally, because of the longer duration of nanosecond laser pulses, more molten material is generated during the ablation process, and granular splashes can be observed around the ablation hole and heat-affected zone. At this point, some of the ablation products are deposited on the hole wall, significantly impacting the laser drilling process and the geometric shape [16,17].

The deposition of ablation products is closely related to environmental pressure [18–20]. Additionally, environmental pressure can also influence ablation efficiency and the diameter of the ablation hole [21]. B. Xia et al. conducted a comparative study on the femtosecond laser drilling process of PMMA materials in vacuum and atmospheric environments. The study found that a vacuum environment is more conducive to plasma discharge, thus increasing ablation efficiency [22]. Wang et al. investigated the effect of an environmental pressure range from 1 Pa to 105 Pa on femtosecond laser ablation of copper, and the results showed that environmental pressure can alter the ablation morphology by changing the focus position [21]. Mutlu et al. studied the ablation behavior of alumina ceramics under different environmental pressures and found that the diameter of the ablation hole increases with the increase in environmental pressure. These findings indicate that a vacuum environment can significantly influence laser ablation behavior [23].

From the perspective of improving ablation efficiency, one of the mainstream approaches is the combined pulse drilling method. This method involves using a continuous laser to create a molten pool on the material surface, followed by the application of a short-pulse laser to ablate the molten pool area. Finally, the molten pool is expelled using the recoil pressure generated by the short-pulse laser from the plasma. Jia et al. demonstrated that the combination of millisecond and nanosecond laser ablation not only improves the roundness of the ablation hole but also reduces the energy required for drilling by an order of magnitude [24]. Another method involves using two sets of nanosecond lasers for hole ablation. Wang et al. investigated the ablation efficiency of dual-nanosecond pulse lasers and found that, in air, the drilling rate of dual-pulse lasers is an order of magnitude higher than that of a single-pulse laser, exceeding 2  $\mu$ m/pulse. The increased drilling efficiency of the dual-pulse method is attributed to the reduction in environmental pressure caused by the second laser beam [25]. However, Noll et al. conducted a detailed analysis of the underlying mechanism, suggesting that the spherical shock wave generated by the first

Appl. Sci. 2025, 15, 848 3 of 13

pulse may expel the atmosphere near the interaction area, leading to a decrease in particle density near the ablation point and the formation of a brief vacuum effect. This, in turn, enhances the interaction between the second laser beam and the target material [26]. In summary, whether by directly altering the environmental pressure or using specific ablation methods to modify it, it is clear that the vacuum environment plays a crucial role in the ablation process of pulse lasers.

Although high-intensity laser technology has found widespread applications in materials processing and scientific research, systematic studies on its ablation behavior in a vacuum environment remain relatively scarce. The existing literature primarily focuses on the interaction between lasers and matter under conventional atmospheric conditions or specific gas environments. However, under vacuum conditions, this interaction mechanism may exhibit distinct characteristics and patterns. Therefore, an in-depth exploration of the ablation behavior of high-intensity lasers in a vacuum environment holds significant theoretical importance and practical application value. The ablative behavior of materials during continuous ablation by nanosecond pulsed lasers has not been thoroughly investigated. This study uses titanium alloy, a typical material, as the research subject and explores the relationship between the ablation depth and volume of titanium alloy under nanosecond laser ablation in a vacuum environment, considering factors such as pulse energy, pulse number, and defocusing distance. The average single-pulse ablation depth and average volume ablation efficiency are measured. Additionally, the three-dimensional morphology of the ablation holes is analyzed, and the ablation plume is captured to support the research findings. The research on the interaction between high-intensity lasers and matter holds significant application value in the fields of materials science, plasma physics, and laser processing technology.

# 2. Experimental Setup

The schematic diagram of the experimental setup is shown in Figure 1. A Nimma-900 laser (Beamtech Optronics Co., Ltd., Beijing, China) was used in the experiment. The maximum single-pulse energy was 900 mJ, with a wavelength of 1064 nm, pulse width of 8 ns, and a repetition rate of 10 Hz. The beam diameter is controlled to 5 mm by an aperture after the laser exits the device. The laser then passes through a 1:9 beam splitter, which reflects 10% of the energy into an energy meter for monitoring, while the remaining 90% is focused on the target using a 300 mm focal length lens; the focal spot of the focusing lens is 300 mm. The beam spot size before the focusing lens is approximately 5 mm in diameter. At the focal point, the beam is focused to a spot size of approximately 300 µm. The target is mounted on a two-dimensional displacement table with a maximum travel distance of 50 mm. The focusing lens is installed on a one-dimensional displacement table that moves along the laser axis to adjust the distance between the lens and the target material. The displacement tables are housed inside a vacuum chamber, which is connected to external control systems. The movement of the tables is precisely controlled by a computer. The vacuum chamber maintains a minimum stable pressure of  $1 \times 10^{-3}$  Pa environment, and all experiments were conducted at this pressure.

Two neodymium magnets and an aperture are installed in front of the target material, with the aperture size carefully selected to allow the laser to pass through. This setup ensures that the focusing lens is not significantly damaged during prolonged ablation. The LEXT OLS5100 laser confocal microscope (Olympus Corporation, Tokyo, Japan) was used as the measurement equipment, which can capture the three-dimensional morphology of ablation holes and measure the depth and volume data. Its measurement accuracy is  $0.15 + L/100~\mu m$  (where L is the measurement depth). The target material used in the experiment was a 2 mm thick TC-4 titanium sheet. Before ablation, the material was

Appl. Sci. 2025, 15, 848 4 of 13

polished with sandpaper up to 600 grit and then wiped with alcohol-soaked cotton to ensure a consistent surface condition throughout the ablation process.

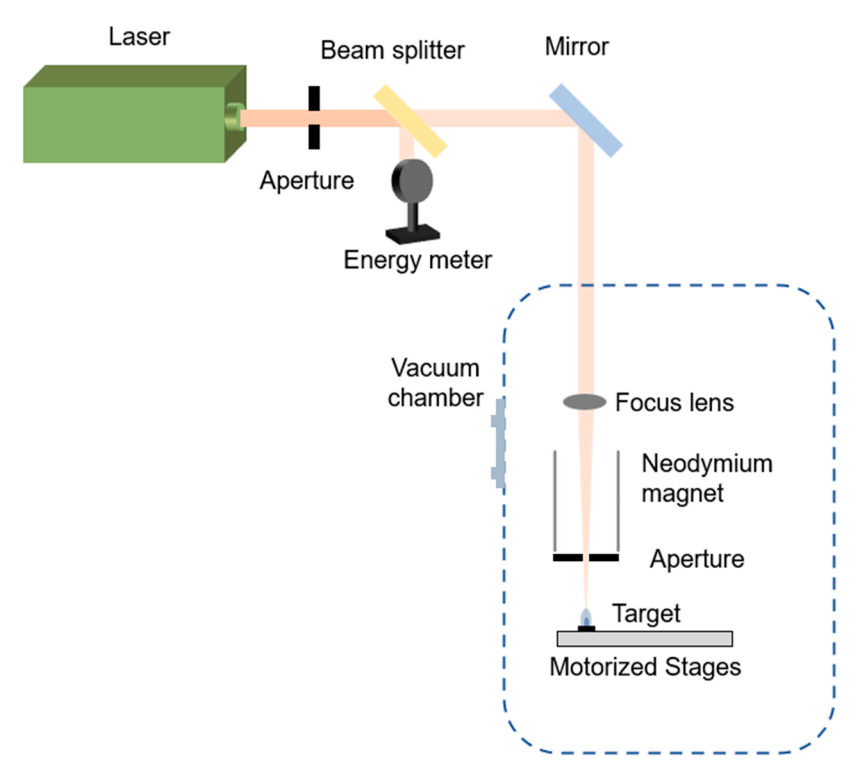


Figure 1. Schematic diagram of experimental setup.

All experiments were performed in triplicate, and the average value was calculated to ensure the reliability of the results.

In the experiment, it was observed that when the focusing lens is near the focal position, the titanium alloy target material with a thickness of 2 mm is easily broken down. Therefore, three titanium alloy targets were polished smooth and secured with fixtures to create a target material with a thickness of 6 mm. This setup was designed to use a thicker layered target to prevent full penetration during ablation, enabling accurate measurement of the ablation depth in the unpenetrated section of the material.

The defocusing distance primarily affects the laser fluence, and the ability of the laser to pierce the target depends on the location where the laser fluence is lowest. When the laser focus is within the target material, the laser fluence remains high across the upper and lower surfaces of the target. In practical experiments, a defocusing distance range of up to 30 mm was achieved, which exceeds the depth of focus (DOF). Based on this, the experiment was designed with a positive defocusing distance, meaning that the focal point is positioned above the target material.

Even if the lens position remains unchanged during the experiment, the diameter of the ablation hole varies due to the non-uniform intensity distribution of the Gaussian beam and the continuous temperature rise during ongoing ablation. The diameter of the ablation hole increases with laser fluence and pulse number [27]. This paper does not address the ablation threshold. The above factors can lead to a discrepancy between the actual ablation hole diameter and the initial laser irradiation area. Using the ablation hole diameter to calculate the energy density may introduce additional errors and complexities. Therefore, to ensure accuracy, we use the spot diameter rather than the ablation hole diameter when calculating the laser energy density to account for the spatial intensity distribution. However, the method for measuring the ablation hole diameter in this study involves assessing the three-dimensional morphology of the hole. The internal diameter

Appl. Sci. 2025, 15, 848 5 of 13

of the ablation hole is defined as the hole diameter, with the material surface serving as the base plane, as shown in Figure 2a. The hole diameter is measured uniformly after 100 pulses, as shown in Figure 2b. Each data point represents an average of multiple measurements in Figure 2b, and the variation between these measurements was minimal.

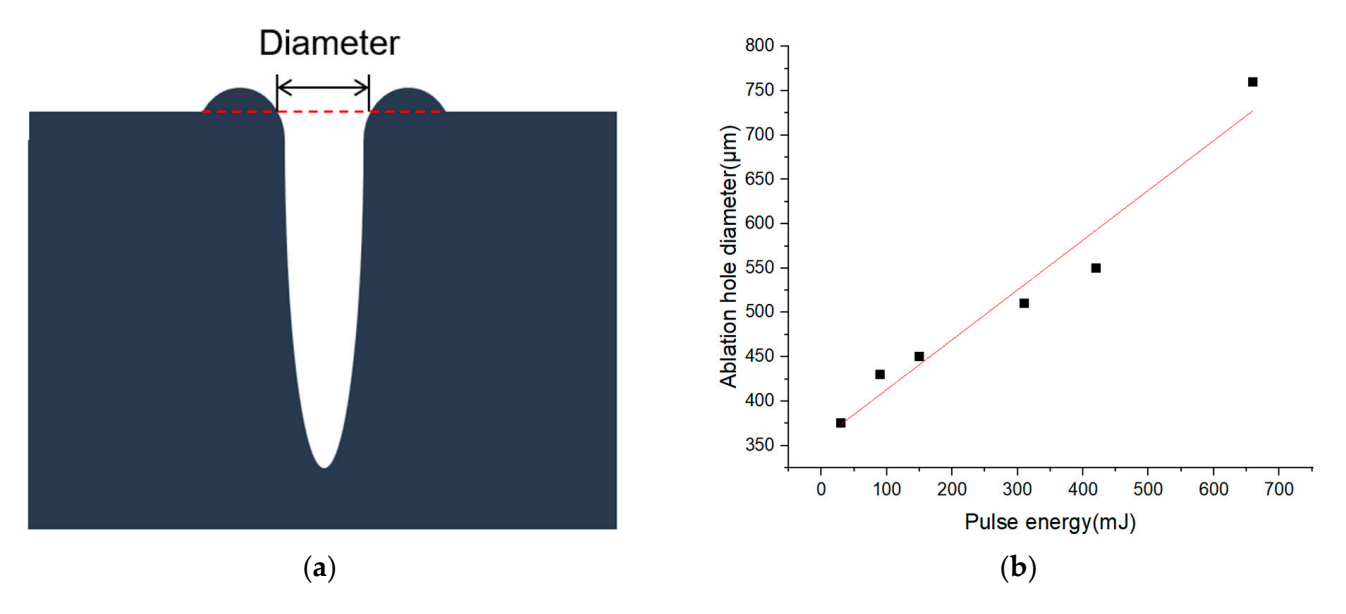


**Figure 2.** (a) Schematic diagram of ablation hole diameter; (b) the change in spot diameter with laser energy.

# 3. Results and Discussion

#### 3.1. Ablation Depth

Firstly, we maintain constant single-pulse energy and vary the defocusing distance by adjusting the lens position, which changes the spot size. This allows us to study the effects of different defocusing distances and pulse numbers on the ablation depth, as shown in Figure 3a.

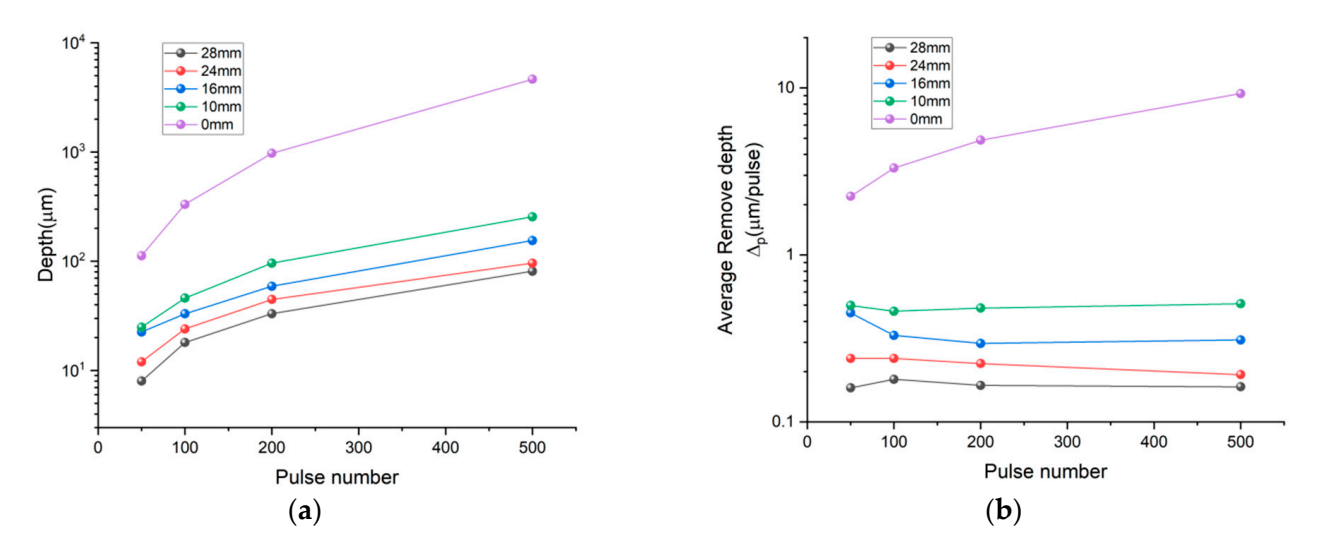


**Figure 3.** (a) Effect of different defocusing amounts on ablation depth; (b) effect of different defocusing amounts on average remove per pulse. The pulse energy used is 660 mJ. The different curves correspond to different distances of lens–target defocusing as indicated.

The defocusing distance primarily affects the diameter of the ablation hole and the distribution of laser energy. As observed in Figure 3a, the ablation depth gradually increases with the number of pulses. However, the ablation depth increases rapidly when the laser

Appl. Sci. 2025, 15, 848 6 of 13

is focused, exceeding 4600  $\mu$ m at 500 pulses. We calculated the average material removal per pulse by dividing the ablation depth by the number of pulses, as shown in Figure 3b. It was found that when the defocusing distance exceeds the focal depth, the average material removal per pulse did not exceed 1  $\mu$ m/pulse. When the laser was focused, our results indicated that the average removal depth increased progressively with the number of pulses, from 2.24  $\mu$ m/pulse (50 pulses) to 9.26  $\mu$ m/pulse (500 pulses), an increase of approximately 4.13 times. This shows that the average removal per pulse is influenced by both the defocusing distance and the pulse number.

To further investigate this phenomenon, the laser drilling capability near the focal point was examined. By fixing the focusing lens and varying the single-pulse energy of the laser, the variation in ablation depth near the focal point with respect to the number of pulses and single-pulse energy was obtained, as shown in Figure 4a. It can be observed that the ablation depth increases with the number of pulses, and the slope gradually increases. When the single-pulse energy of the laser is 150 mJ (energy density is  $4.13 \, \text{J/cm}^2$ ), there is almost no nonlinear increase in ablation depth. However, when the single-pulse energy reaches 310 mJ (energy density is  $8.54 \, \text{J/cm}^2$ ), a clear nonlinear increase in ablation depth is evident. The nonlinear increase in ablation depth becomes more pronounced with increasing energy density.

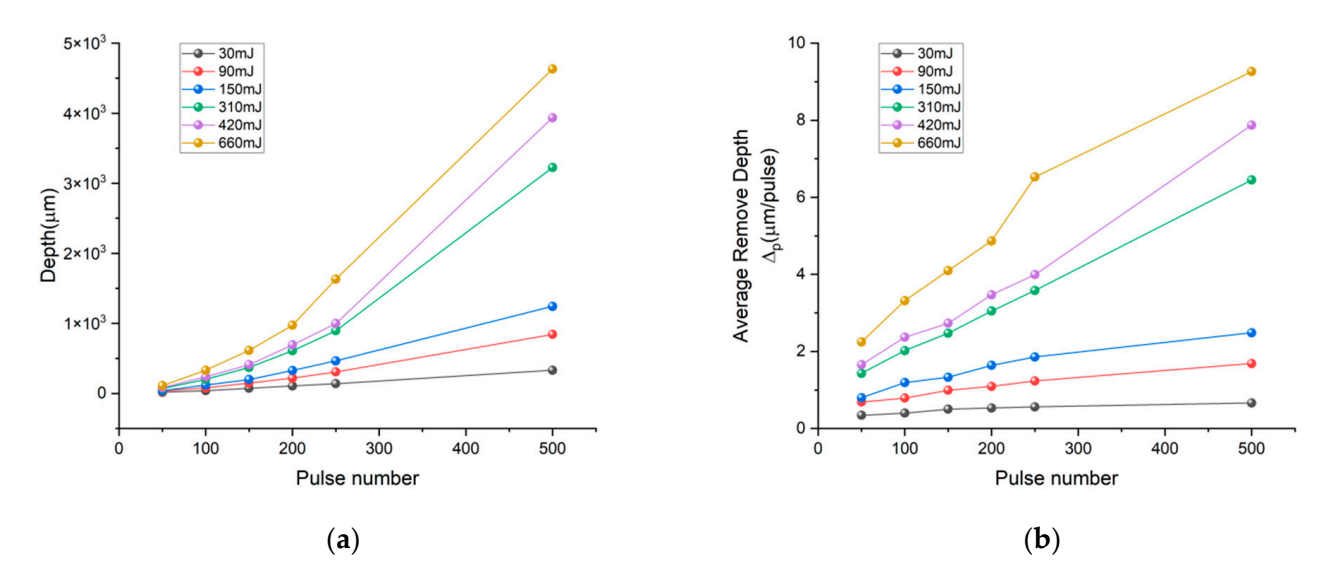


**Figure 4.** (a) Effect of different single-pulse energies on ablation depth; (b) effect of different single-pulse energies on average removed per pulse. The different curves correspond to different single-pulse energy as indicated.

The average material removal per pulse was calculated, as shown in Figure 4b. It can be seen that at the focal position, when the laser energy is below 150 mJ, the average material removal per pulse hardly increases with the number of pulses. However, when the laser energy exceeds 310 mJ, the average material removal per pulse increases with the number of pulses.

#### 3.2. Ablation Volume and Efficiency

The ablation depth can reflect the longitudinal development process of the ablation holes, but it does not accurately represent the true ablative efficiency. Therefore, we further measured the volume ablation parameters of the ablation holes. As shown in Figure 5, when the single pulse energy is 660 mJ, the total ablation volume at various defocusing distances is obtained by adjusting the position of the lens.

Appl. Sci. 2025, 15, 848 7 of 13

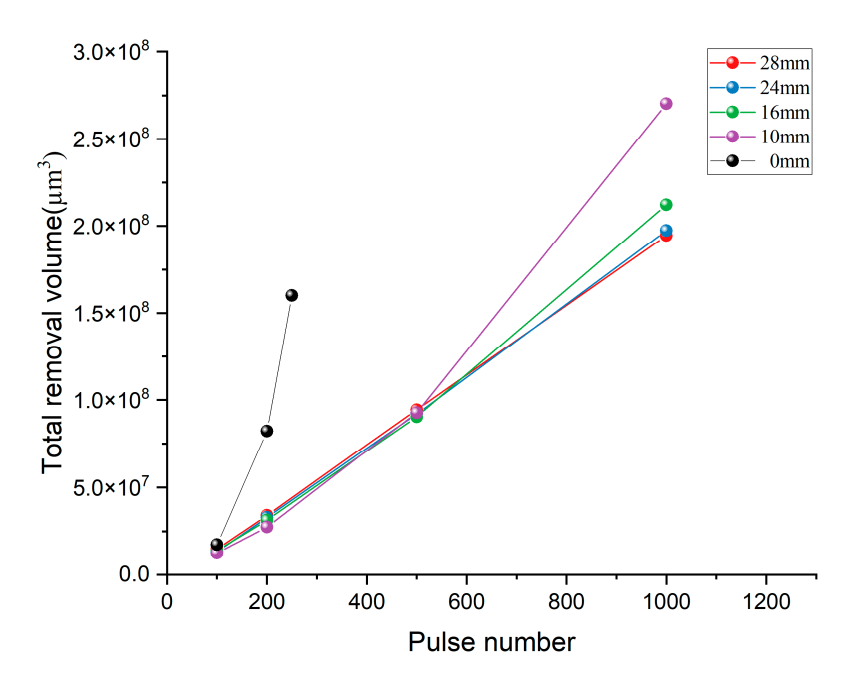


**Figure 5.** Relationship between the ablation volume and the number of pulses; the laser energy remains constant at 660 mJ. The different curves correspond to different distances of lens–target defocusing as indicated.

It can be observed that when the pulse energy is less than 500 pulses, the ablation volume remains almost unchanged with the defocusing amount. As the defocusing distance decreases, the ablation area becomes smaller, but the power density increases, resulting in an increase in ablation depth. This factor compensates for the effect of the reduced ablation area. Therefore, we speculate that the primary material removal mechanism in this case is gasification. We believe that the gasification observed during the laser ablation of the metal surface is evaporation rather than boiling. This is because, in the laser ablation process, laser energy is rapidly focused onto a small area of the metal surface, causing a sharp rise in temperature. Due to the extremely rapid heating, atoms on the metal surface gain sufficient energy to transition directly from solid or liquid to gas, which is characteristic of evaporation. This differs from conventional boiling, which typically occurs when the entire liquid reaches its boiling point, accompanied by bubble formation and growth. Thus, the high energy density and rapid heating in laser ablation result in a direct phase change, more consistent with evaporation. In this case, the ablation volume is primarily determined by the single-pulse energy. When the number of laser pulses reaches 1000, the ablation volumes at different defocusing distances begin to diverge. We speculate that this is due to the more concentrated heat deposition during the laser ablation process as the ablation area decreases, leading to higher temperatures and an increase in laser absorption [28].

Subsequently, the lens was adjusted to a position near the focal point, and the effect of single-pulse energy on the average removal volume was measured, as shown in Figure 6a. The "average removal volume" is defined as the ablation volume divided by the number of pulses, while the "average removal efficiency" is calculated by dividing the average single-pulse ablation volume by the single-pulse energy. Due to limitations of the measurement equipment, ablation holes with a depth-to-diameter ratio greater than 4 could not be measured. Therefore, the number of pulses was reduced, and the average single-pulse ablation volume was measured as a function of energy density and pulse number, ranging from 50 to 250 pulses.

Appl. Sci. 2025, 15, 848 8 of 13

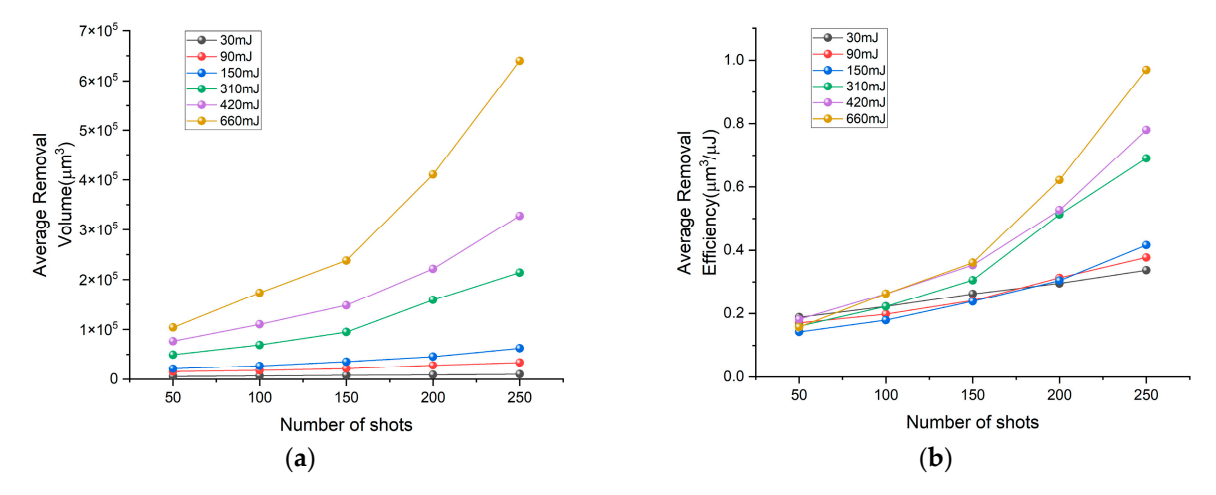


**Figure 6.** (a) Effect of single-pulse energy on average single pulse-ablation volume; (b) effect of single-pulse energy on average volume ablation efficiency. The different curves correspond to different single-pulse energies as indicated.

The average volume ablation efficiency of the target material was calculated as a function of single-pulse energy, as shown in Figure 6b. When the single-pulse energy ranged from 30 to 150 mJ, the average volume ablation efficiency increased slowly. With an increasing number of pulses, the ablation data exceed the volume ablation efficiency observed in the nanosecond laser ablation of titanium alloys under atmospheric conditions [29]. In Figure 6, it can be observed that both the average removal volume and average removal efficiency continue to rise with the number of pulses. This trend may initially seem inconsistent with the results shown in Figure 3a, where the ablation depth starts to plateau at higher pulse numbers. The discrepancy can be attributed to the experimental setup in Figure 6, where the lens is positioned near the focal point, ensuring a higher energy density in the laser-irradiated area. At this focal position, the increased laser energy density likely leads to a more efficient material removal process. Furthermore, the vacuum environment in which these experiments were conducted may contribute to this trend by facilitating localized heat accumulation and reducing plasma shielding effects due to the absence of convective cooling. These conditions promote sustained high temperatures and greater energy absorption over successive pulses. Previous studies have shown that repeated laser irradiation can induce surface microstructural changes, reducing reflectivity and thereby enhancing laser energy absorption efficiency [30]. This phenomenon is particularly significant at high pulse energies and may explain why the ablation efficiency observed in Figure 6 does not decrease as rapidly with increasing pulse numbers, as would be expected under atmospheric conditions. Taken together, these factors—the high energy density near the focal point, the vacuum environment's effect on heat accumulation and plasma dissipation, and the reduced reflectivity due to surface changes—contribute to the differences observed in Figure 6.

## 3.3. Ablation Plume

Several factors contribute to the nonlinear increase in laser ablation depth. First, when the laser interacts with the target material, the temperature of the material rises. For metals, the laser absorption rate typically increases with temperature due to changes in the behavior of free electrons and surface properties, which enhance the efficiency of laser energy absorption [28]. Second, the vacuum environment minimizes atmospheric interactions, enabling more efficient energy transfer to the material surface [31]. Third, as the depth of the ablation hole increases, laser reflection within the irradiation area leads to multiple reflections on the walls of the ablation hole, eventually refocusing at the bottom,

Appl. Sci. 2025, 15, 848 9 of 13

which results in an increased absorption of laser energy [32]. Additionally, in atmospheric environments, heat dissipation during nanosecond laser drilling occurs primarily through convection. In contrast, in vacuum environments, convection is absent, and heat dissipation occurs solely through thermal radiation and thermal diffusion.

To investigate the underlying causes of the observed phenomenon, a series of experiments were conducted to capture ablation plumes under varying conditions, as shown in Figure 7. The integration time, aperture, and distance used for plume image capture were set to 0.5 s, 35 cm, and f6.4, respectively. A laser energy of 100 mJ was used throughout the ablation plume experiments, and the target material was positioned at the focal point. Figure 7a presents the initial plasma image generated upon the laser's first irradiation of the target. Next, a hole was drilled into the target, allowed to cool, and then irradiated with the plasma inside the hole, as depicted in Figure 7c. A comparison between these two images reveals that when the laser is focused inside the hole, a slightly higher amount of plasma is generated, indicating that the hole enhances the laser absorption rate. After approximately 210 pulses of repeated irradiation with a 1 Hz laser, the plasma image, shown in Figure 7b, displayed a significantly larger amount of plasma, suggesting an increased laser absorption rate during this phase. Furthermore, when a 10 Hz laser was used for continuous ablation of the target, as shown in Figure 7d, bright linear streaks were observed, which may indicate the presence of ejected molten material. These features resemble patterns typically associated with molten particles during laser ablation. Given that the vaporization latent heat of titanium alloy greatly exceeds its melting latent heat, the emergence of molten splashing material is undoubtedly the primary factor contributing to the sharp increase in ablation efficiency. As seen in Figure 7d, due to the excessively high intensity of the plasma, it was not possible to clearly distinguish the ejected material. Therefore, a neutral density filter was added in the areas with higher plasma intensity, which reduces the light intensity by 100 times. This effectively prevented CMOS saturation, allowing the ejected material to be distinguished.

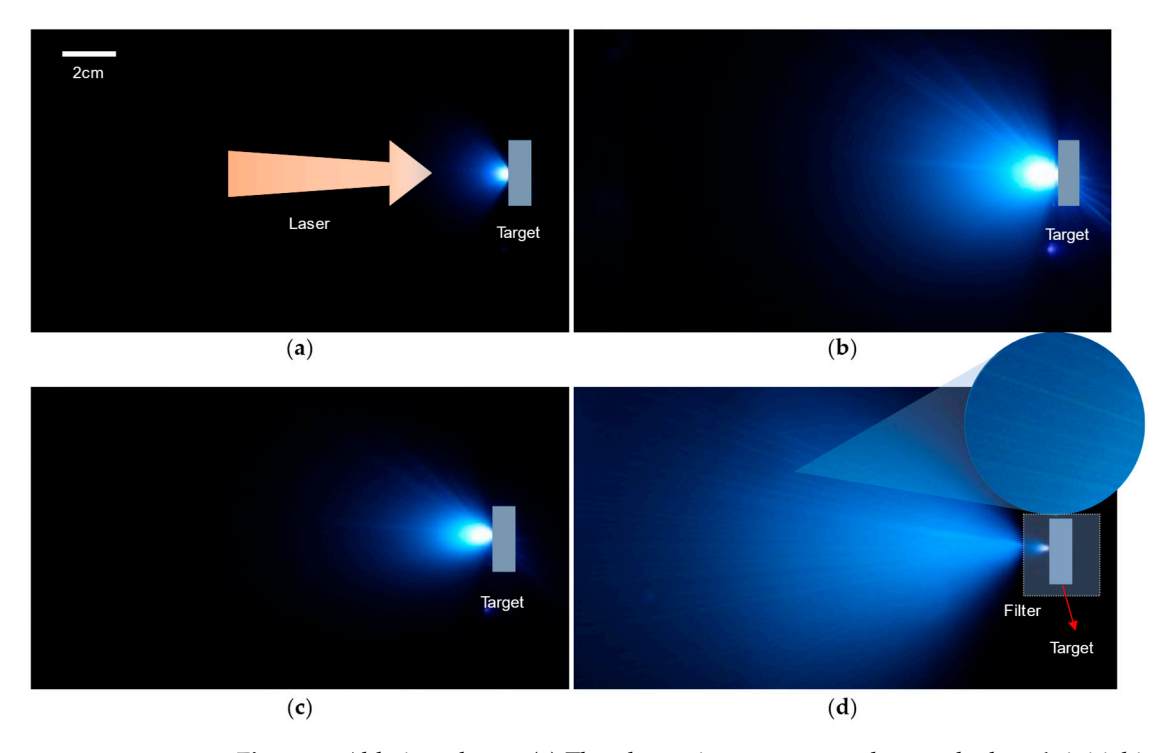


**Figure 7.** Ablation plume. (a) The plasma image generated upon the laser's initial irradiation on the target; (b) the plume image produced by repeated ablation of about 210 times with a 1 Hz laser; (c) the ablation plume produced by irradiating a laser through a small hole; (d) the plume image produced by repeated ablation with a 10 Hz laser.

Since the experiment was conducted in a vacuum environment, heat dissipation primarily occurred through radiation and conduction, rather than convection. As a result, localized heat accumulation may have occurred in the laser-irradiated area. Previous studies have shown that repeated laser irradiation can induce microstructural changes on the material surface, which reduce its reflectivity and consequently increase the absorption of laser energy [30]. This enhanced absorption may enable subsequent laser pulses to heat the area more effectively, thereby improving ablation efficiency. This observation is consistent with our experimental results, where the ablation efficiency of laser-induced craters is significantly higher in the vacuum environment, likely due to the combined effects of localized heat accumulation and increased absorption. This mechanism is similar to the enhancement observed in multi-pulse laser ablation [33].

### 3.4. Ablation Morphology

Finally, the ablation morphology of titanium alloy under different parameters was photographed to observe the deposition of ablation products on the target material surface during laser drilling in a vacuum environment.

Two typical morphology images were selected. Figure 8a shows the ablation morphology with a single-pulse energy laser of 660 mJ, a defocusing distance of 16 mm (hole size of 1020  $\mu$ m), and a pulse number of 500. A regular recast layer surrounding the ablation pit is observed. Figure 8b shows the ablation morphology with a single-pulse energy laser of 660 mJ, a pulse number of 250, and a defocusing distance of 0 mm. Obvious recast layers were observed in both experimental conditions. When the defocusing distance was 16 mm, the bottom of the ablation hole was very smooth, and the recast layer was very uniform. Based on the previously mentioned average single-pulse ablation depth of 0.31  $\mu$ m/pulse, it can be concluded that the material removal mode under these conditions was primarily vaporization. When the single-pulse energy was 660 mJ, and the target was positioned at the focal point, clear signs of titanium alloy melting were observed around the ablation hole. A large amount of recast layer surrounded the hole, and the shape of the ablation hole was conical. A smaller aperture facilitated the generation of higher recoil pressure, which, in turn, made it easier to expel the melt. This was also one of the reasons for the nonlinear increase in ablation depth.

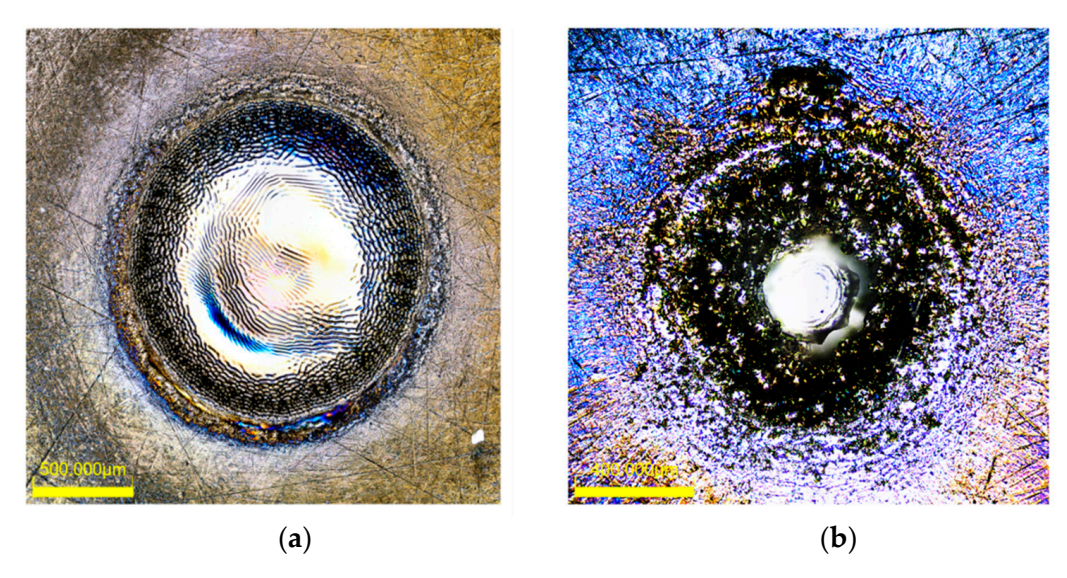


**Figure 8.** Ablation morphology under different nanosecond pulse laser parameters: (a) pulse energy 660 mJ, hole diameter 1020  $\mu$ m, number of shots 500; (b) pulse energy 660 mJ, hole diameter 375  $\mu$ m, number of shots 250.

# 4. Conclusions

The researchers conducted repeated ablation experiments using high-intensity lasers in a vacuum environment for high-efficiency laser drilling. The variation in ablation depth and volume with power density, pulse number, and defocus was investigated, and the average single-pulse ablation depth and average volume ablation efficiency were calculated. The results indicate that, in a vacuum environment, the absence of convective heat dissipation significantly reduces heat loss at the bottom of the ablation hole. When continuous ablation is performed at a repetition rate of 10 Hz, the titanium alloy exhibits an enhanced ablation mechanism, similar to the effect observed in pulsed laser drilling. The high repetition rate generates a continuous liquid surface at the bottom of the ablation hole, which is ejected under the scouring action of the plasma. This mechanism increases the average single-pulse ablation depth of the nanosecond laser by more than four times. The measured average single-pulse ablation volume reached 0.97  $\mu$ m $^3/\mu$ J. The combination of the vacuum environment and multi-pulse nanosecond laser significantly improves both ablation efficiency and hole quality.

The study of the interaction between high-intensity lasers and matter holds significant application value in the fields of materials science, plasma physics, and laser processing technology. However, current research on the ablation behavior of high-intensity lasers in a vacuum environment remains limited. Delving deeper into this field not only aids in understanding the fundamental mechanisms of laser–matter interactions but also propels the advancement of related technologies. For instance, grasping the ablation characteristics of high-intensity lasers in vacuum conditions will significantly propel technological progress in areas such as spacecraft surface treatment, precision manufacturing, and the development of novel materials. Therefore, conducting a systematic study on this topic not only bears great theoretical significance but also exerts a profound influence on practical engineering applications.

**Author Contributions:** All authors contributed to the study conception and design. Conceptualization, Y.W. and J.Y.; methodology, J.Y. and H.G.; formal analysis, Y.W. and H.G.; investigation, Y.W., H.G., B.D., S.L., Q.C., S.W. and T.Z.; resources, Q.C. and D.W.; data curation, H.G.; writing—original draft preparation, H.G.; writing—review and editing, H.G., B.D. and Y.W.; supervision, S.L. and D.W.; project administration, S.L. and Q.C.; funding acquisition, Y.W. and J.Y. All authors have read and agreed to the published version of the manuscript.

**Funding:** This work was supported by the State Key Laboratory of Laser Propulsion & Application Independent Research Project (SKLLPA-202206).

**Institutional Review Board Statement:** Not applicable.

**Informed Consent Statement:** Not applicable.

Data Availability Statement: Data is contained within the article.

Conflicts of Interest: The authors declare no conflicts of interest.

# References

- 1. Yilbas, B.S.; Sahin, A.Z. Laser Pulse Optimization for Practical Laser Drilling. Opt. Lasers Eng. 1994, 20, 311–323. [CrossRef]
- 2. Rohde, H.; Meiners, E. Trepan Drilling of Fuel Injection Nozzles With a TEM(00) Nd: YAG Slab Laser. *J. Laser Appl.* **1996**, *8*, 95–101. [CrossRef]
- 3. Mcnally, C.A.; Folkes, J.; Pashby, I.R. Laser drilling of cooling holes in aeroengines: State of the art and future challenges. *Mater. Sci. Technol.* **2004**, *20*, 805–813. [CrossRef]
- 4. Gautam, G.D.; Pandey, A.K. Pulsed Nd: YAG laser beam drilling: A review. Opt. Laser Technol. 2018, 100, 183–215. [CrossRef]
- 5. Zhang, S.; Fan, Y.; Huang, Y.; Yang, X.; Zhang, M.; Luo, J.; Deng, G.; Zhou, Q.; Song, H.; Wang, Y. Improvement of the surface condition of laser-drilled holes via a dual-wavelength double-pulse train. *Opt. Laser Technol.* **2023**, *157*, 108681. [CrossRef]

6. Li, W.; Zhang, G.; Huang, Y.; Rong, Y. Drilling of CFRP plates with adjustable pulse duration fiber laser. *Mater. Manuf. Process.* **2021**, *36*, 1256–1263. [CrossRef]

- 7. Jackson, M.J.; O'neill, W. Laser micro-drilling of tool steel using Nd: YAG lasers. *J. Mater. Process. Technol.* **2003**, 142, 517–525. [CrossRef]
- 8. Wang, C.-S.; Hsiao, Y.-H.; Chang, H.-Y.; Chang, Y.-J. Process Parameter Prediction and Modeling of Laser Percussion Drilling by Artificial Neural Networks. *Micromachines* **2022**, *13*, 529. [CrossRef]
- 9. Li, Z.; Yang, Z.; Jia, X.; Wang, C.; Li, K.; Shen, H.; Duan, J. Numerical analysis of the effect of temporal and/or spatial shaping on the ms/ns combined pulse laser drilling performance of alumina ceramic. *Opt. Laser Technol.* **2023**, *164*, 109481. [CrossRef]
- Wang, H.; Liu, J.; Xu, Y.; Wang, X.; Ren, N.; Ren, X.; Hu, Q. Experimental characterization and real-time monitoring for laser percussion drilling in titanium alloy using transverse electric field assistance and/or lateral air blowing. *J. Manuf. Process.* 2021, 62, 845–858. [CrossRef]
- 11. Xia, K.; Ren, N.; Lin, Q.; Li, T.; Gao, F.; Yang, H.; Song, S. Experimental investigation of femtosecond laser through-hole drilling of stainless steel with and without transverse magnetic assistance. *Appl. Opt.* **2021**, *60*, 1399–1410. [CrossRef] [PubMed]
- 12. Yuan, C.G.; Pramanik, A.; Basak, A.K.; Prakash, C.; Shankar, S. Drilling of titanium alloy (Ti6Al4V)—A review. *Mach. Sci. Technol.* **2021**, 25, 637–702. [CrossRef]
- 13. Schulz, W.; Eppelt, U.; Poprawe, R. Review on laser drilling I. Fundamentals, modeling, and simulation. *J. Laser Appl.* **2013**, 25, 012006. [CrossRef]
- 14. Phillips, K.C.; Gandhi, H.H.; Mazur, E.; Sundaram, S.K. Ultrafast laser processing of materials: A review. *Adv. Opt. Photonics* **2015**, 7, 684–712. [CrossRef]
- 15. Tao, S.; Wu, B.X.; Lei, S.T. Study of laser beam propagation in micro-holes and the effect on femtosecond laser micromachining. *J. Appl. Phys.* **2011**, *109*, 123506. [CrossRef]
- 16. Salleo, A.; Sands, T.; Genin, F.Y. Machining of transparent materials using an IR and UV nanosecond pulsed laser. *Appl. Phys. A Mater. Sci. Process.* **2000**, *71*, 601–618. [CrossRef]
- 17. Liu, D.; Kong, D.; Miao, Z.; Zhang, X. Simulation and experimental investigation on nano-second pulsed laser drilling of titanium alloy. *High Power Laser Part. Beams* **2018**, *30*, 069001.
- 18. Vorobyev, A.Y.; Guo, C.L. Enhanced energy coupling in femtosecond laser-metal interactions at high intensities. *Opt. Express* **2006**, *14*, 13113–13119. [CrossRef]
- 19. Döring, S.; Richter, S.; Heisler, F.; Ullsperger, T.; Tünnermann, A.; Nolte, S. Influence of ambient pressure on the hole formation in laser deep drilling. *Appl. Phys. A Mater. Sci. Process.* **2013**, *112*, 623–629. [CrossRef]
- 20. Kononenko, T.V.; Klimentov, S.M.; Konov, V.I.; Dausinger, F. Effect of air breakdown on short-pulsed laser drilling. In Proceedings of the International Conference on Lasers, Applications and Technologies, St. Petersburg, Russia, 11–15 May 2005.
- 21. Wang, Q.; Chen, A.; Li, S.; Qi, H.; Qi, Y.; Hu, Z.; Jin, M. Influence of ambient pressure on the ablation hole in femtosecond laser drilling Cu. *Appl. Opt.* **2015**, *54*, 8235–8240. [CrossRef]
- 22. Xia, B.; Jiang, L.; Li, X.; Yan, X.; Zhao, W.; Lu, Y. High aspect ratio, high-quality micro-holes in PMMA: A comparison between femtosecond laser drilling in air and in vacuum. *Appl. Phys. A Mater. Sci. Process.* **2015**, *119*, 61–68. [CrossRef]
- 23. Mutlu, M.; Kacar, E.L.; Akman, E.R.; Akkan, C.K.; Demir, P.; Demir, A. Effects of The Laser Wavelength on Drilling Process of Ceramic Using Nd: YAG Laser. *J. Laser Micro Nanoeng.* **2009**, *4*, 84–88. [CrossRef]
- 24. Jia, X.; Zhu, G.; Zhang, Y.; Chen, Y.; Wang, H.; Shan, P.; Aleksei, K.; Zhu, X. Laser processing of alumina ceramic by spatially and temporally superposing the millisecond pulse and nanosecond pulse train. *Opt. Express* **2020**, *28*, 676–684. [CrossRef]
- 25. Wang, X.; Michalowski, A.; Walter, D.; Sommer, S.; Kraus, M.; Liu, J.; Dausinger, F. Laser drilling of stainless steel with nanosecond double-pulse. *Opt. Laser Technol.* **2009**, *41*, 148–153. [CrossRef]
- 26. Noll, R.; Sattmann, R.; Sturm, V.; Winkelmann, S. Space- and time-resolved dynamics of plasmas generated by laser double pulses interacting with metallic samples. *J. Anal. At. Spectrom.* **2004**, *19*, 419–428. [CrossRef]
- 27. Bonse, J.; Baudach, S.; Krüger, J.; Kautek, W.; Lenzner, M. Femtosecond laser ablation of silicon–modification thresholds and morphology. *Appl. Phys. A* **2002**, *74*, 19–25. [CrossRef]
- 28. Shen, N.; Bude, J.D.; Ly, S.; Keller, W.J.; Rubenchik, A.M.; Negres, R.; Guss, G. Enhancement of laser material drilling using high-impulse multi-laser melt ejection. *Opt. Express* **2019**, 27, 19864–19886. [CrossRef] [PubMed]
- 29. Zhao, J.; Zhu, Z.; Xu, Y.; Song, X.; Wang, Y.; Peng, H.; Wang, Y.; Zuo, J.; Shu, X.; Yin, A. Nanosecond Laser Ablation of Ti–6Al–4V under Different Temperature. *Appl. Sci.* **2020**, *10*, 4657. [CrossRef]
- 30. Kovalev, O.B.; Zaitsev, A.V. Modeling of the free-surface shape in laser cutting of metals. 2. model of multiple reflection and absorption of radiation. *J. Appl. Mech. Tech. Phys.* **2005**, *46*, 9–13. [CrossRef]
- 31. Gusarov, A.V.; Kruth, J.P. Modelling of radiation transfer in metallic powders at laser treatment. *Int. J. Heat Mass Transf.* **2005**, *48*, 3423–3434. [CrossRef]

32. Garrelie, F.; Champeaux, C.; Catherinot, A. Study by a Monte Carlo simulation of the influence of a background gas on the expansion dynamics of a laser-induced plasma plume. *Appl. Phys. A* **1999**, *69*, 45–50. [CrossRef]

33. Schneider, M.; Berthe, L.; Fabbro, R.; Muller, M. Measurement of laser absorptivity for operating parameters characteristic of laser drilling regime. *J. Phys. D Appl. Phys.* **2009**, *41*, 155502. [CrossRef]

**Disclaimer/Publisher's Note:** The statements, opinions and data contained in all publications are solely those of the individual author(s) and contributor(s) and not of MDPI and/or the editor(s). MDPI and/or the editor(s) disclaim responsibility for any injury to people or property resulting from any ideas, methods, instructions or products referred to in the content.